Motion and Parameter Estimation of a Free-Floating Space Object from Range Data for Motion Prediction

Ulrich Hillenbrand and Roberto Lampariello
Institute of Robotics and Mechatronics
German Aerospace Center (DLR)
82234 Weßling, Germany
{*Ulrich.Hillenbrand,Roberto.Lampariello*}*@dlr.de*

***Abstract*— A method is investigated for the motion estimation and the model identification of a free-floating target in space. Motion estimation relies on range data measurements, which are here simulated for analyzing the method. The work is motivated by the necessity to provide an efficient long-term motion prediction algorithm, in the order of 100 seconds, to support planning of complex maneuvers or tracking during long phases without observation.**

The method is evaluated for different scenarios of range measurements and for a series of target motions, including translation and rotation or pure rotation about different axes, which may represent typical scenarios for tumbling objects in orbit.

8th International Symposium on Artificial Intelligence, Robotics and Automation in Space (iSAIRAS 2005).

I. Introduction

This work investigates a method for the motion estimation and for the dynamic model identification of a free-floating target in space. The motion parameter estimation is performed from range data as may be measured by stereo vision or a laser range sensor. The goal of this procedure is to finally allow long-term motion prediction of the target, in the order of 100 seconds, with the identified dynamic model. In the estimation procedure, it is assumed that nothing is initially known about the inertial properties, the geometry, or the motion of the target.

The present study is distinct from others aiming at short-term prediction to the next observation, parameter identification, where the goal is the accuracy of the identified parameters, and pose estimation or tracking of a known object, where high-level model knowledge can be used.

Long-term prediction is useful for the case in which observation is not possible for a long time (e.g. occlusions, limited communication to ground) or in which a task which requires long-term planning is of interest (such as autonomous grasping).

The task is divided into three subtasks: motion estimation from range data, parameter identification from the motion estimates, and prediction with the identified parameters. Simulated range data will be used to analyze the method. Different scenarios of range data measurements are considered. The computation time and the robustness to noise and to parameter excitation of the method are addressed. An empirical error statistics is also presented.

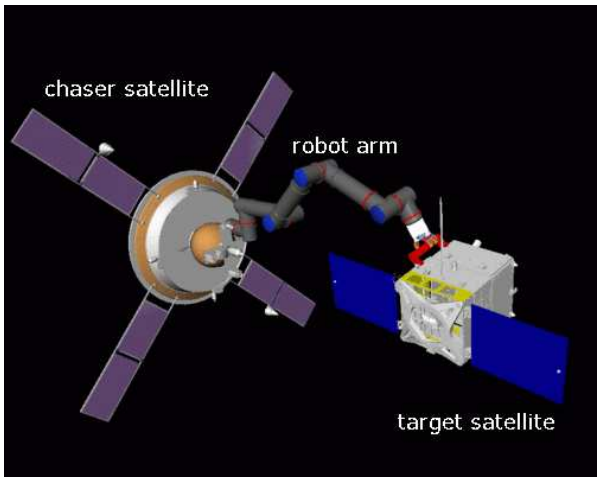

Fig. 1. TECSAS scenario: a robot mounted on a chaser satellite grasping a target satellite

II. Bibliography

Previous work on related problems includes that of [1], [2], [3], and [4]. In the first, an extended Kalman filter is used to track and predict the motion of a target with known inertial parameters. The prediction of the target motion, which is approximated to a constant linear and angular velocity, is performed on-line, but only for a few seconds of duration.

In [2] the inertial parameter identification problem is also treated with a Kalman filter. The estimates, however, are not validated for their suitability for long-term prediction. Moreover, the assumptions made on the range data available are rather strong, in that measurements from the complete target surface are required at every observation time.

In [3], which also aims at motion prediction, the analytical solution to the Euler equations is used. The predicted time span, however, is still short compared to the observation time. Moreover, no treatment of translation and of noise (except quantization noise) is included. Furthermore, only the case of known point correspondences without occlusion is considered.

Finally in [4], the authors investigate the Hough transform for pose tracking with an emphasis on computational speed rather than on estimation accuracy. No long-term prediction can be based on their estimation results, and the

object is assumed to be geometrically known.

III. Methods

In this section, the range-data generation for the purpose of this study is addressed. Thereafter, the motion estimation and prediction procedures are described. First, motion estimation from the range data provides incremental translation and rotation estimates of the target. These are then used as input to the identification of a suitable set of parameters for the dynamic model of the target. Finally, prediction of target motion is performed with the dynamic model thus identified.

In this section, time t often takes discrete values in intervals of one second. For ease of reading, we then drop the units and simply write $t = 0, 1, 2, \ldots$ in the equations.

A. Data generation

The target object that we have simulated for this study is a geometrically abstracted version of a satellite that is planned to be used in the TECSAS mission; see Fig. 1. It is a box with sides 450×450×600 mm and two solar panels attached to opposite sides of 560 mm length each.

We consider three different scenarios of range-data measurements of the target.

1) The visible fraction of a set of 100 points, randomly and uniformly distributed over the target surface, are sensed at each observation time, with the point correspondence across time known.
2) As above, but with the point correspondence across time unknown.
3) The visible fraction of 10,000 points are sensed, randomly and uniformly distributed over the target surface, and without point correspondence across time, that is, independently drawn at each observation time.

Scenarios 1 and 2 could be realized by stereo processing of at least two synchronous camera images. Special interest points may then be tracked over time or local correspondences may be searched across the images of two successive time frames. If inter-time correspondence is reliable, the first scenario is realized. If inter-time correspondence is unreliable and, hence, not enforced, the second scenario is realized. In scenario 3, there are no corresponding points in the data. It is then necessary for successful motion estimation that the target surface is represented by a rather dense set of points. This scenario may be realized by a stereo camera system, a laser scanner, or any other range sensor that is capable of producing dense measurements.

For each scenario of measurement, we have simulated 10 trajectories of the target over 100 seconds. Single-view range data are generated from target poses at time intervals of one second, taking occlusion and surface slant into account. For our trajectories, between 20% and 60% of the points were visible at each time. We added independent isotropic Gaussian noise with a 5 mm standard deviation to each visible point. This level of noise is rather high. We have chosen it to emphasize the relative ability of the measurement scenarios to cope with unreliable data.

B. Motion estimation

Scenario 1 requires estimation of a rotation $\mathbf{R}$ and a translation $\mathbf{t}$ that match the data points $\{\mathbf{r}^1(t-1), \mathbf{r}^2(t-1), \ldots, \mathbf{r}^N(t-1)\}$ measured at time $t-1$ to the corresponding data points $\{\mathbf{r}^1(t), \mathbf{r}^2(t), \ldots, \mathbf{r}^N(t)\}$ measured at time t. That is, we seek a rotation $\mathbf{R}(t-1,t)$ and a translation $\mathbf{t}(t-1,t)$ such that

$$\mathbf{r}^i(t) = \mathbf{R}(t-1,t)\,\mathbf{r}^i(t-1) + \mathbf{t}(t-1,t) + \eta(t-1,t)\ , \quad (1)$$

$i = 1, 2, \ldots, N$, where $\eta(t-1,t)$ describes the added measurement errors (noise) at times $t-1$ and t. We hence have to minimize the match error

$$E_1(\mathbf{R},\mathbf{t}) = \sum_{i=1}^{N} ||\mathbf{r}^i(t) - \mathbf{R}\,\mathbf{r}^i(t-1) - \mathbf{t}||^2 \quad (2)$$

for each time step $t-1 \mapsto t$ of one second, where $||\ \cdot\ ||$ denotes the Euclidean norm. The minimizer of $E_1(\mathbf{R},\mathbf{t})$ is the sought estimate of the rotation and translation for that time step,

$$[\hat{\mathbf{R}}(t-1,t), \hat{\mathbf{t}}(t-1,t)] = \arg\min_{[\mathbf{R},\mathbf{t}]} E_1(\mathbf{R},\mathbf{t})\ . \quad (3)$$

Solving (3) is a linear least-squares problem that has a closed-form solution. Different formulations of this problem exist [6]. We have decided for a formulation where the rotations are represented by unit quaternions [5]. Briefly, minimizing $E_1(\mathbf{R},\mathbf{t})$ can be shown to be equivalent to maximizing the quadratic form

$$F(\mathbf{q}) = \mathbf{q}^T\,\mathbf{D}\,\mathbf{q} \quad (4)$$

over the unit quaternions $\mathbf{q}$, where $\mathbf{D}$ is a symmetric real 4×4 matrix that depends on the data. Let the data points $\mathbf{r}^i(t) = [r_1^i(t), r_2^i(t), r_3^i(t)]$, $i = 1, 2, \ldots, N$. Then

$$\mathbf{D} = \begin{bmatrix} S_{11}+S_{22}+S_{33} & S_{23}-S_{32} & S_{31}-S_{13} & S_{12}-S_{21} \\ S_{23}-S_{32} & S_{11}-S_{22}-S_{33} & S_{12}+S_{21} & S_{31}+S_{13} \\ S_{31}-S_{13} & S_{12}+S_{21} & -S_{11}+S_{22}-S_{33} & S_{23}+S_{32} \\ S_{12}-S_{21} & S_{31}+S_{13} & S_{23}+S_{32} & -S_{11}-S_{22}+S_{33} \end{bmatrix}, \quad (5)$$

with

$$S_{jk} = \sum_{i=1}^{N} r_j^i(t-1)\,r_k^i(t)\ . \quad (6)$$

The maximizer of (4),

$$\hat{\mathbf{q}} = \arg\max_{||\mathbf{q}||=1} F(\mathbf{q})\ , \quad (7)$$

is given by the normalized eigenvector corresponding to the largest (most positive) eigenvalue of D.[1] This eigenvector may be obtained in closed form or through an iterative procedure. The sought rotation estimate $\hat{\mathbf{R}}(t-1,t)$ is represented by $\hat{\mathbf{q}}$. The sought translation estimate $\hat{\mathbf{t}}(t-1,t)$

[1] There are two such eigenvectors, one being the negative of the other. Both represent the same rotation.

is then given by

$$\hat{\mathbf{t}}(t-1,t) = \frac{1}{N}\left[\sum_{i=1}^{N}\mathbf{r}^i(t) - \hat{\mathbf{R}}(t-1,t)\sum_{i=1}^{N}\mathbf{r}^i(t-1)\right] , \tag{8}$$

i.e., it takes the rotated data centroid at time $t-1$ into the data centroid at time t.

If the point correspondences are unknown, as in scenario 2, things are slightly more complicated. In fact, every false correspondence between a point at time $t-1$ and a point at time t is effectively an outlier that cannot be modeled by the error function (2). If false correspondences are not removed, the estimation error incurred from minimizing $E_1(\mathbf{R},\mathbf{t})$ may be arbitrarily large. The least-squares solution above has thus to be made robust by a mechanism for selecting pairs of corresponding points.

Selection of corresponding point candidates is simplified here by the smoothness and limited speed of the target motion. We have employed a robust M-estimator, that is,

$$[\hat{\mathbf{R}}(t-1,t), \hat{\mathbf{t}}(t-1,t)] = \arg\min_{[\mathbf{R},\mathbf{t}]} E_1^{\mathrm{r}}(\mathbf{R},\mathbf{t}) , \tag{9}$$

with the robust error function

$$E_1^{\mathrm{r}}(\mathbf{R},\mathbf{t}) = \sum_{i=1}^{N(t-1)}\sum_{j=1}^{N(t)} e_{ij}(\mathbf{R},\mathbf{t}) , \tag{10}$$

$$e_{ij}(\mathbf{R},\mathbf{t}) = \begin{cases} ||\mathbf{r}^j(t) - \mathbf{R}\,\mathbf{r}^i(t-1) - \mathbf{t}||^2 \\ \qquad \text{if } ||\mathbf{r}^j(t) - \mathbf{R}\,\mathbf{r}^i(t-1) - \mathbf{t}|| < s, \\ s^2 \\ \qquad \text{else.} \end{cases} \tag{11}$$

In (10), $N(t-1)$ and $N(t)$ denote the number of data points at times $t-1$ and t, respectively. In (11), the scale parameter s determines the range of correspondences effectively made between points at successive time frames. The minimization problem (9) is solved by an iteratively-reweighted-least-squares (IRLS) procedure, with the scale s decreasing with progressive iteration. At the start, s should be equal to the expected motion distance of points on the target surface. The final iterations should be performed with s being equal to the expected measurement error. We have set s to twice the error standard deviation for the final iterations. The iteration may stop after a predefined number of steps or according to a convergence criterion.

The IRLS procedure is here somewhat similar to the iterative-closest-point (ICP) algorithm [7]. However, ICP does not have a scale parameter to control the range of point correspondences.

Scenario 3 is processed the same way as scenario 2, but with a larger final value for the scale s. This is preferable in the absence of true point correspondences, where the final estimate must be based on averaging across accidental point correspondences. In fact, s should be larger than the minimum expected distance between data points on the surface. Furthermore, there are some implementation differences to scenario 2 in order to adapt the algorithm to the higher number of data points. In particular, its run time is only linear in the number of data points.

C. Dynamic parameter identification

The dynamic model consists of the equations of motion of a single free-floating rigid body. The sought parameters normally consist of the center-of-mass position and the inertia matrix. However, due to the non-identifiability of the latter for the present case of a non-actuated free-floating body, these parameters are found with respect to an arbitrary constant factor. Moreover, in the case of rotation about a stationary axis, nothing can be inferred about the inertia, and the center-of-mass position can be identified only in the components orthogonal to the axis. However, since the aim here is prediction of the trajectory, non-identifiability of parameters is not a problem.

It is well known that the equations of motion of a free-floating rigid body can be solved analytically. The solutions for the angular velocities are periodic functions (when neglecting energy dissipation) which can, in principle, be approximated with a Fourier series expansion. The drawback of this approach is that the observation time must be at least as long as the period of the component with the lowest frequency, which is typically very long. This reason motivated resorting to the identification of a dynamic model.

The identification problem is divided into two parts, since the rotational motion is decoupled from the translational motion in the dynamic formulation.

1) Inertia and initial angular velocity: The differential equations for the rotational motion of a torque-free rigid body can be written as

Kinematics:

$$\dot{\mathbf{q}} = \begin{bmatrix} \dot{q}_0 \\ \dot{q}_1 \\ \dot{q}_2 \\ \dot{q}_3 \end{bmatrix} = \frac{1}{2}\begin{bmatrix} -\omega_1 q_1 - \omega_2 q_2 - \omega_3 q_3 \\ \omega_1 q_0 + \omega_3 q_2 - \omega_2 q_3 \\ \omega_2 q_0 - \omega_3 q_1 + \omega_1 q_3 \\ \omega_3 q_0 + \omega_2 q_1 - \omega_1 q_2 \end{bmatrix} , \tag{12}$$

Dynamics:

$$\mathbf{I}\,\dot{\boldsymbol{\omega}} + (\boldsymbol{\omega} \times \mathbf{I}\,\boldsymbol{\omega}) = 0 , \tag{13}$$

having used the quaternion parameterization of the body rotation, $\mathbf{q} = [q_0, q_1, q_2, q_3]^T$. In equation (12), $[\omega_1, \omega_2, \omega_3]^T$ represent the components of the angular velocity in the inertial frame; in equation (13), $\boldsymbol{\omega}$ represents the angular velocity and $\mathbf{I}$ the inertia matrix in the body frame. Note that for the free-floating case the actuation term on the right-hand side is zero (orbital disturbances are here neglected, although they can be included in the dynamic model at a later stage).

The time integration of these equations for a time interval of one second then provides the following outcome:

$$\mathbf{q}(t-1,t) \;=\; \int_{t-1}^{t} \dot{\mathbf{q}}\, dt \tag{14}$$

$$\boldsymbol{\omega}(t-1,t) \;=\; -\int_{t-1}^{t} \mathbf{I}^{-1}\,(\boldsymbol{\omega} \times \mathbf{I}\boldsymbol{\omega})\, dt \tag{15}$$

with initial conditions $\mathbf{q}(0)$, $\boldsymbol{\omega}(0)$.

The unknowns in our identification procedure are the six inertial parameters in the matrix $\mathbf{I}$ and the initial conditions for the integration. However, for the quaternion we can assume that the initial conditions are the identity quaternion, with no loss of generality. The identification procedure then consists in constructing a nonlinear error function in the remaining nine unknown parameters,

$$\mathbf{p} \;=\; [\mathbf{I}_{11}, \mathbf{I}_{22}, \mathbf{I}_{33}, \mathbf{I}_{12}, \mathbf{I}_{13}, \mathbf{I}_{23}, \omega_1(0), \omega_2(0), \omega_3(0)]^T \;. \tag{16}$$

The error function is defined here as the Euclidean distance in the three-dimensional space of the quaternion vector components:

$$E_2(\mathbf{p}) \;=\; \sum_{t=1}^{100} \| \, \mathbf{q}_{\mathrm{v}}(t-1, t; \mathbf{p}) - \hat{\mathbf{q}}_{\mathrm{v}}(t-1, t) \, \|^2 \;, \tag{17}$$

where $\mathbf{q}_{\mathrm{v}} = [q_1, q_2, q_3]$ and $\hat{\mathbf{q}}_{\mathrm{v}} = [\hat{q}_1, \hat{q}_2, \hat{q}_3]$ derives from the rotation estimates computed as explained in sec. III-B.

A nonlinear optimization problem is then defined as

$$\hat{\mathbf{p}} = \arg\min_{\mathbf{p}} E_2(\mathbf{p}) \tag{18}$$

solved here by sequential quadratic programming. Note that, for physical consistency, the inequality constraints

$$\mathbf{I}_{11} + \mathbf{I}_{22} > \mathbf{I}_{33} \;, \quad \mathbf{I}_{22} + \mathbf{I}_{33} > \mathbf{I}_{11} \;, \quad \mathbf{I}_{33} + \mathbf{I}_{11} > \mathbf{I}_{22} \tag{19}$$

must be enforced.

The inertial parameters, in fact, appear linearly in the equations, such that one can also write the dynamic equations (13) as

$$\boldsymbol{\Phi}(\boldsymbol{\omega}, \dot{\boldsymbol{\omega}}) \mathbf{p}_{\mathrm{lin}} \;=\; \boldsymbol{\tau} \;, \tag{20}$$

where matrix $\boldsymbol{\Phi}$ is generally termed the regressor matrix, column matrix $\mathbf{p}_{\mathrm{lin}}$ contains the unknown inertia parameters, and column matrix $\boldsymbol{\tau}$ the actuation to the system (zero for the case of a free-floating body). Note that this linear formulation of the estimation problem needs to be modified to allow for the linear dependence of the six equations [2]. By setting one of the unknowns to some arbitrary constant, the system can be reduced to five unknowns with a non-zero right-hand side, allowing the rest of the parameters to be found.

It is important to note, however, that in the formulation (20) both angular velocity and acceleration measurements are necessary in the regressor matrix $\boldsymbol{\Phi}$ and in $\boldsymbol{\tau}$. Since the observed visual data consists of displacements per time frame, therefore an approximation to velocity, these would have to be differentiated to provide the required accelerations. In the nonlinear formulation, on the other hand, the observed data are used directly. Furthermore, in (20), both the regressor matrix $\boldsymbol{\Phi}$ and actuation vector $\boldsymbol{\tau}$ contain data and therefore noise. As such, a resolution of equation (20) does not lead to a true maximum-likelihood estimate. For these reasons, the use of the nonlinear formulation is thought to be more adequate for this problem.

[2]If the equations were not linearly dependent the only solution would be the trivial one, $\mathbf{p}_{\mathrm{lin}} = 0$. This also shows that for this case the inertia parameters can only be identified with respect to an arbitrary constant.

However, an analytical estimate of uncertainty cannot be provided for the nonlinear formulation. We have thus resorted to a purely empirical statistical analysis, as shown in the section on experimental results.

The proposed method is further developed to treat outliers in the motion estimates as follows. A first identification run is performed on the untreated estimates. The latter are then scanned through and compared at each time step to the outcome of the first identification run. The 5 worst motion estimates are then removed and the dynamic parameters identified based on the remaining estimates.

The initial guess used for the parameters is

$$\begin{aligned}\mathbf{p}_{\mathrm{init}} \;=\; [&1000\,\mathrm{kg\,m^2}, 1000\,\mathrm{kg\,m^2}, 1000\,\mathrm{kg\,m^2}, \\ &10\,\mathrm{kg\,m^2}, 10\,\mathrm{kg\,m^2}, 10\,\mathrm{kg\,m^2}, \\ &\omega_1^*, \omega_2^*, \omega_3^*]^T \;.\end{aligned} \tag{21}$$

Five different initial guesses are taken for the last three parameters (angular velocity initial condition $\boldsymbol{\omega}^*$) from the first five motion estimates in each trajectory. The best identification result, as judged by the residual error, is then selected for the prediction which follows. The method normally converges to a solution in a few seconds.

2) Center-of-mass velocity and initial position: The translational motion of the target is described by the motion of its center of mass. In this study, we assume no external force and, therefore, a constant translational velocity for the center of mass.[3] Its position in time is given by

$$\mathbf{c}(t) = t\,\mathbf{v} + \mathbf{c}(0) \;, \tag{22}$$

with the center-of-mass velocity $\mathbf{v}$ and position at time zero $\mathbf{c}(0)$, which are the unknowns of the problem. Since the center of mass is a point on the rigidly moving target, its motion must also follow the target rotation and translation, that is,

$$\mathbf{c}(t) = \mathbf{R}(t-1, t)\,\mathbf{c}(t-1) + \mathbf{t}(t-1, t) \;. \tag{23}$$

Plugging in the rotation and translation estimates for each time step $t-1 \mapsto t$ computed as described in sec. III-B, we arrive at

$$t\,\mathbf{v} + \mathbf{c}(0) = \hat{\mathbf{R}}(t-1, t)\;[(t-1)\,\mathbf{v} + \mathbf{c}(0)] + \hat{\mathbf{t}}(t-1, t) \;. \tag{24}$$

This equation is obtained for each of the 100 observation time steps, leading to an over-determined system for the unknowns $\mathbf{v}$ and $\mathbf{c}(0)$. Treating it as a linear least-squares problem, we have to solve

$$[\hat{\mathbf{v}}, \hat{\mathbf{c}}(0)] = \arg\min_{[\mathbf{v}, \mathbf{c}(0)]} E_3(\mathbf{v}, \mathbf{c}(0)) \;, \tag{25}$$

with the error function

$$\begin{aligned}E_3(\mathbf{v}, \mathbf{c}(0)) = \sum_{t=1}^{100} ||&t\,\mathbf{v} + \mathbf{c}(0) - \hat{\mathbf{t}}(t-1, t) \\ &- \hat{\mathbf{R}}(t-1, t)\;[(t-1)\,\mathbf{v} + \mathbf{c}(0)]\,||^2 \;.\end{aligned} \tag{26}$$

[3]The general formulation of the problem, however, can be extended to cover other motions.

The minimizer is given by

$$\begin{bmatrix} \hat{\mathbf{v}} \\ \hat{\mathbf{c}}(0) \end{bmatrix} = \mathbf{\Phi}^{+} \begin{bmatrix} \hat{\mathbf{t}}(0,1) \\ \hat{\mathbf{t}}(1,2) \\ \vdots \\ \hat{\mathbf{t}}(99,100) \end{bmatrix} , \tag{27}$$

where $\mathbf{\Phi}^{+}$ is the pseudo-inverse of the 300×6 regressor matrix $\mathbf{\Phi}$.

In a somewhat more rigorous treatment, one would formulate the joint nonlinear least-squares problem for the inertial and center-of-mass parameters. However, this higher-dimensional, nonlinear optimization problem may in practice yield less accurate results, due to the increasing problems with local minima of the cost function.

D. Motion prediction

As stated above, the final goal of this procedure is to perform motion prediction of a given point on the target (this point may be chosen by an operator or by some intelligent algorithm). For this we need to integrate the equations of motion with the parameter estimates:

$$\tilde{\mathbf{q}}(t) \;=\; \int_0^t \dot{\mathbf{q}}\, dt \tag{28}$$

$$\tilde{\boldsymbol{\omega}}(t) \;=\; -\int_0^t \hat{\mathbf{I}}^{-1}\,(\boldsymbol{\omega} \times \hat{\mathbf{I}}\boldsymbol{\omega})\, dt \tag{29}$$

with initial conditions $\mathbf{q}(0)$, $\hat{\boldsymbol{\omega}}(0)$ and then arrive at the position of the chosen point from the equation:

$$\tilde{\mathbf{r}}_{\mathrm{p}}(t) = t\,\hat{\mathbf{v}} + \mathbf{R}(\tilde{\mathbf{q}}(\mathbf{t}))(\mathbf{r}_{\mathrm{p}}(0) - \hat{\mathbf{c}}(0)) + \hat{\mathbf{c}}(0) \tag{30}$$

where $\mathbf{R}(\tilde{\mathbf{q}}(\mathbf{t}))$ is given by the integration in equation (28) and $\hat{\mathbf{v}}$ and $\hat{\mathbf{c}}(0)$ by the identification procedure in sec. III-C.2 respectively.

IV. Experiments

A. Sample trajectories

The trajectories were chosen to cover different possible target motions, typical of free-floating bodies in orbit. These were chosen to have a maximum rotational velocity of 4 deg/s and a maximum translational velocity of 1 cm/s in any of the three orthogonal directions of Euclidean space.[4] Furthermore, the motions range between pure rotation about a stationary axis and rotation about time-varying axes, as well as with zero or nonzero translational velocities. Finally, two different sets of inertial parameters were selected, as shown in table I.

B. Motion estimation

In Fig. 2, we show a sample trajectory of the target together with the associated motion estimates. Plotted are rotations $\mathbf{R}(t-1,t)$ and translations $\mathbf{t}(t-1,t)$ for the observation time intervals $t-1 \mapsto t$ of one second. The rotations are given in canonical coordinates $\alpha = [\alpha_1, \alpha_2, \alpha_3] \in \mathbb{R}^3$. Their relation to a rotation $\mathbf{R}$ is given by

$$\mathbf{R} = \exp(\alpha_1\,\mathbf{\Lambda}_1 + \alpha_2\,\mathbf{\Lambda}_2 + \alpha_3\,\mathbf{\Lambda}_3)\ , \tag{31}$$

with $\mathbf{\Lambda}_1, \mathbf{\Lambda}_2, \mathbf{\Lambda}_3$ being infinitesimal rotations about the world x-, y-, and z-axes, respectively. In fact, $||\alpha||$ is the angle and $\alpha/||\alpha||$ the (oriented) axis of the rotation $\mathbf{R}$. The translations are given in vector components $\mathbf{t} = [t_1, t_2, t_3]$ along the world x-, y-, and z-axes. We have computed error measures for the rotation estimates $\hat{\mathbf{R}}(t-1,t)$ and the translation estimates $\hat{\mathbf{t}}(t-1,t)$ at each time step $t-1 \mapsto t$. Since the temporal dependence is irrelevant in this section, we here drop the temporal arguments for simplicity.

For the errors of rotation estimates, we have computed the Euclidean distance in the space of canonical coordinates between estimated rotation $\hat{\mathbf{R}}$ and true rotation $\mathbf{R}$,

$$e_{\mathrm{rot}}(\hat{\mathbf{R}}, \mathbf{R}) = ||\alpha(\hat{\mathbf{R}}) - \alpha(\mathbf{R})||\ . \tag{32}$$

It is interesting to note that, for the small rotations here encountered, the distance (32) gives to a good approximation the angle of the rotation difference $\mathbf{R}\,\hat{\mathbf{R}}^{-1}$ between $\hat{\mathbf{R}}$ and $\mathbf{R}$. The errors of translation estimates $\hat{\mathbf{t}}$ are measured by the Euclidean distance to the true translation vector $\mathbf{t}$,

$$e_{\mathrm{trans}}(\hat{\mathbf{t}}, \mathbf{t}) = ||\hat{\mathbf{t}} - \mathbf{t}||\ . \tag{33}$$

Note, however, that the translation errors depend upon the rotation errors through eq. (8).

From 10 runs through each of the 10 trajectories with 100 frames per trajectory we have obtained a total of 10,000 motion estimates for each of the three scenarios. Figures 3, 4, and 5 show frequency histograms of the rotation and translation errors. The size of rotations and translations present in the data sequences may be measured by $e_{\mathrm{rot}}(\mathrm{Id}, \mathbf{R}) = ||\alpha||$ and $e_{\mathrm{trans}}(0, \mathbf{t}) = ||\mathbf{t}||$, respectively. The corresponding histograms are shown in Fig. 6. Note that these histograms would be the error distributions, if we had simply guessed that the target is not moving at all.

One may compare the probability density of rotation estimates to an isotropic Gaussian in the space of canonical coordinates centered on the true rotation, that is,

$$p_{\mathrm{rot}}(\hat{\mathbf{R}}) \propto \exp\left(-\frac{e_{\mathrm{rot}}(\hat{\mathbf{R}}, \mathbf{R})^2}{2\,\sigma_{\mathrm{rot}}^2}\right)\ . \tag{34}$$

Note that isotropy is a reasonable assumption, if the density should describe all kinds of motion of the target relative to the observer. Likewise, the density of translation estimates may be compared to

$$p_{\mathrm{trans}}(\hat{\mathbf{t}}) \propto \exp\left(-\frac{e_{\mathrm{trans}}(\hat{\mathbf{t}}, \mathbf{t})^2}{2\,\sigma_{\mathrm{trans}}^2}\right)\ . \tag{35}$$

The corresponding histograms for e_{rot} and e_{trans} in Figs. 3, 4, and 5 should then compare to the error densities

$$\rho(e) \propto e^2\,\exp\left(-\frac{e^2}{2\,\sigma^2}\right)\ . \tag{36}$$

The standard deviations $\sigma = \sigma_{\mathrm{rot}}, \sigma_{\mathrm{trans}}$ are estimated from the rotation errors $e = e_{\mathrm{rot}}$ and the translation errors $e =$

[4]Note that the velocities are taken relative to the orbital frame of reference, which rotates with the orbital angular velocity, which also equals the observation frame.

Trajectory	Inertia	Center-of-mass velocity	Angular velocity
1	$\mathbf{I}_1$	$\mathbf{v}_1$	ω_1
2	$\mathbf{I}_1$	$\mathbf{v}_1$	ω_2
3	$\mathbf{I}_1$	$\mathbf{v}_1$	ω_3
4	$\mathbf{I}_1$	$\mathbf{v}_1$	ω_4
5	$\mathbf{I}_1$	$\mathbf{v}_1$	ω_5
6	$\mathbf{I}_1$	$\mathbf{v}_1$	ω_6
7	$\mathbf{I}_2$	$\mathbf{v}_1$	ω_3
8	$\mathbf{I}_2$	$\mathbf{v}_1$	ω_4
9	$\mathbf{I}_1$	$\mathbf{v}_2$	ω_5
10	$\mathbf{I}_2$	$\mathbf{v}_2$	ω_6

Inertia [kg m^2]	$\mathbf{I}_1 =$	5665.46	54.24	145.11	$\mathbf{I}_2 =$	700.0	0.0	0.0
		54.24	3032.99	-123.19		0.0	900.0	0.0
		145.11	-123.19	7067.23		0.0	0.0	500.0

Center-of-mass velocity [cm/s]	$\mathbf{v}_1 = (0.005, 0.010, 0.0032)$	$\mathbf{v}_2 = (0.0, 0.0, 0.0)$
Angular velocity [rad/s]	$\boldsymbol{\omega}_1 = (0.04, 0.04, 0.04)$	$\boldsymbol{\omega}_2 = (0.0, 0.04, 0.0)$
	$\boldsymbol{\omega}_3 = (0.0, 0.0, 0.04)$	$\boldsymbol{\omega}_4 = (0.001, 0.005, 0.04)$
	$\boldsymbol{\omega}_5 = (0.01, 0.001, 0.02)$	$\boldsymbol{\omega}_6 = (0.002, 0.01, 0.001)$

TABLE I

TRAJECTORY SET DEFINITION

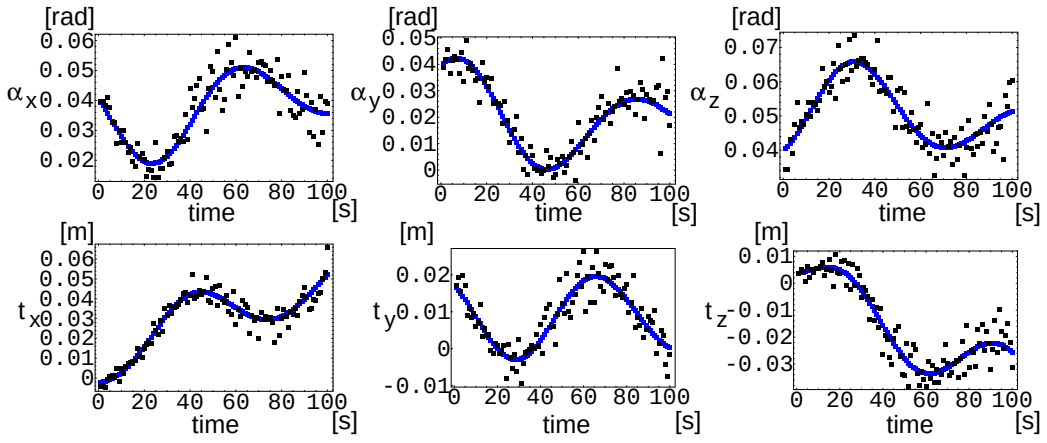

Fig. 2. Sample trajectory (trajectory 1 of table I, blue dots) and associated motion estimates (black dots). The rotations (top row) are plotted in canonical coordinates, the translations (bottom row) in vector components.

e_{trans}, respectively, as

$$\sigma = \sqrt{\frac{n}{\sum_{i=1}^{n} 1/e_i^2}} \ , \tag{37}$$

assuming a sample of n estimates. These standard deviations are given in Figs. 7, 8, and 9 for the three scenarios, along with a graph showing the quality of the Gaussian fit.

As one would have expected, scenario 1 produces the highest accuracy. In fact, it represents the optimum achievable for motion estimation given the data distribution. The rotation-estimate errors are seen to be Gaussian, while the translation-estimate errors have a longer tail than a Gaussian with the same standard deviation. In scenario 2, the rotation-estimate error is Gaussian as well, with a roughly $3/2$-fold increase in σ_{rot}. The distribution of translation-estimate errors broadens by roughly the same factor, again decaying slower than a Gaussian. Scenario 3 is the most difficult one. The main change is in the quality of rotation estimates, whose error distribution now exhibits a non-Gaussian tail as well. The translation-error distribution is even longer-tailed than in scenario 2.

A deviation of an error distribution from a Gaussian may compromise assumptions implicitly made in formulating a cost function for parameter identification; cf. eqs. (17) and (26). Indeed, a cost function that is quadratic in the errors of motion estimates is justified by the maximum-likelihood criterion of parameter estimation only for Gaussian errors.

On a Pentium 4 at 2.4 GHz running under Linux, processing of a single observation step took around 5 ms for scenario 1, 25 ms for scenario 2, and 3 s for scenario 3.

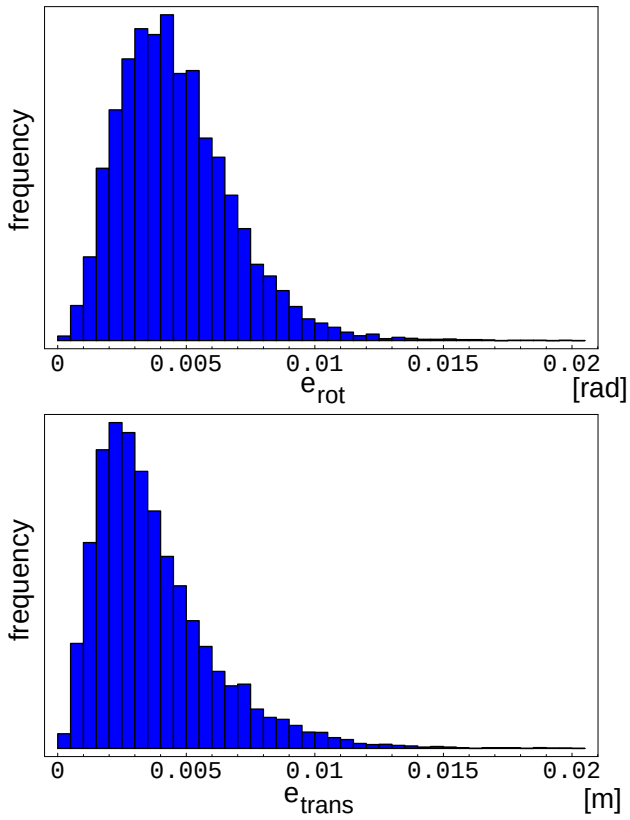

Fig. 3. Histograms of estimation error for rotation (top) and translation (bottom) for the test-data sequences and scenario 1.

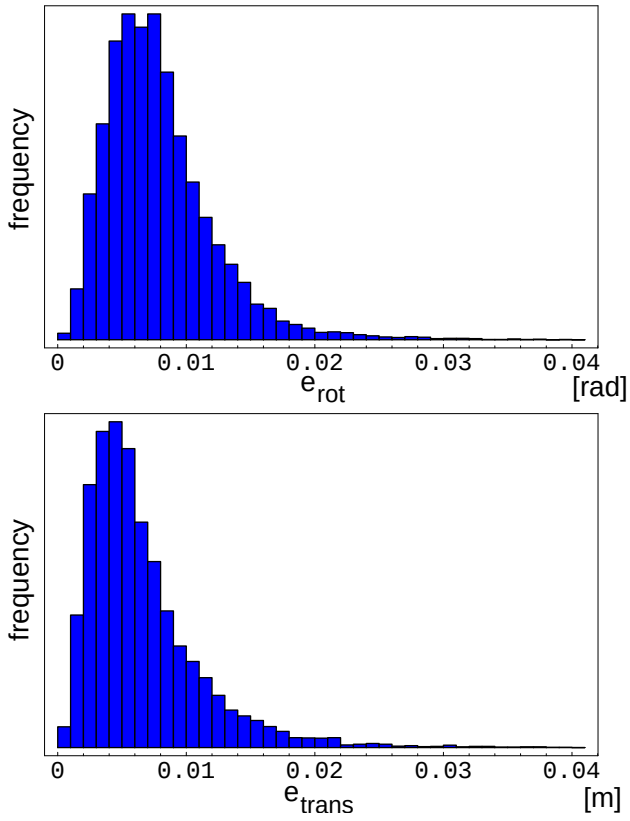

Fig. 4. Histograms of estimation error for rotation (top) and translation (bottom) for the test-data sequences and scenario 2.

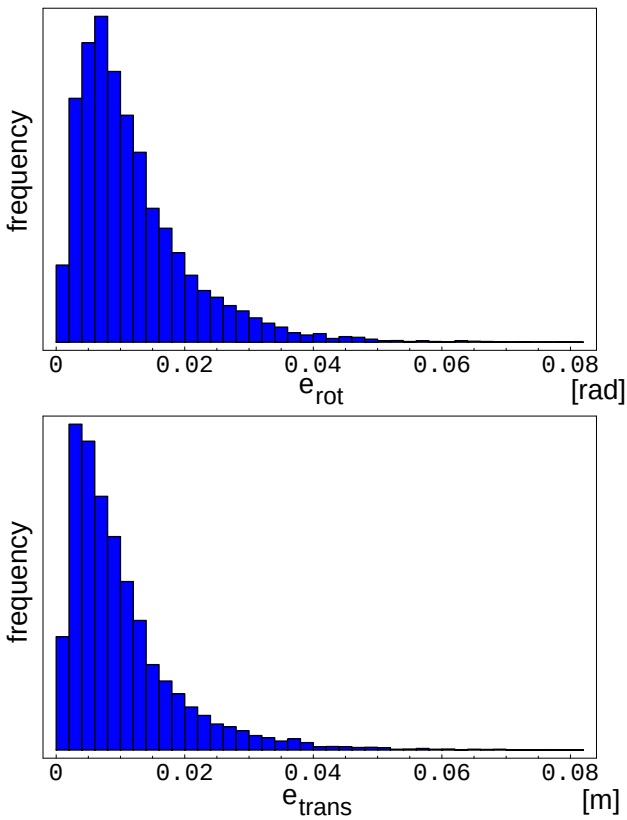

Fig. 5. Histograms of estimation error for rotation (top) and translation (bottom) for the test-data sequences and scenario 3.

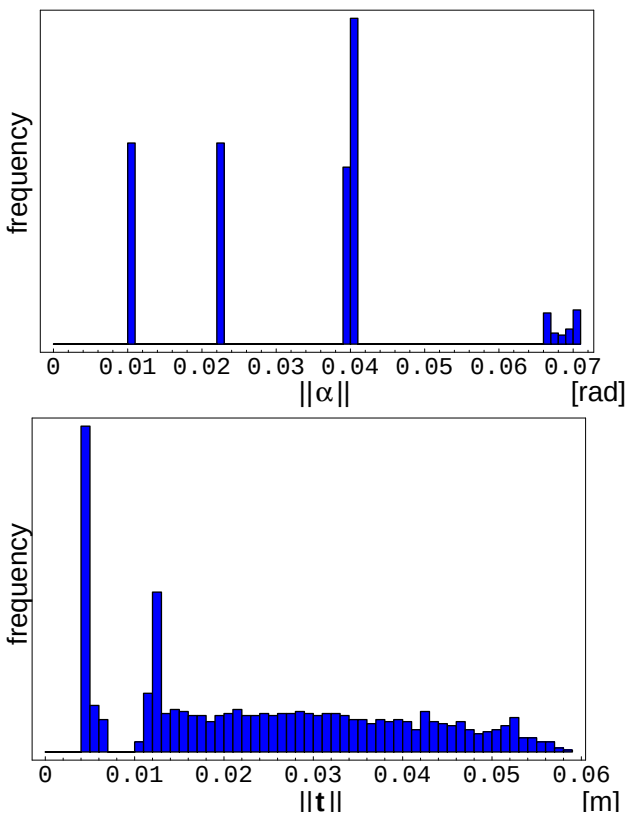

Fig. 6. Histograms of size of rotations (top) and translations (bottom) in the test-data sequences.

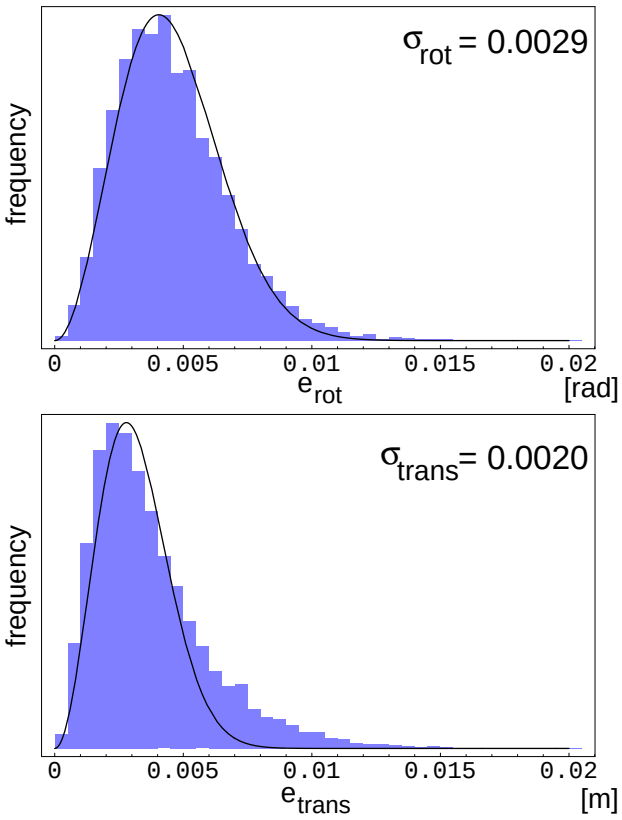

Fig. 7. Gaussian fits of estimation error for rotation (top) and translation (bottom) for the test-data sequences and scenario 1.

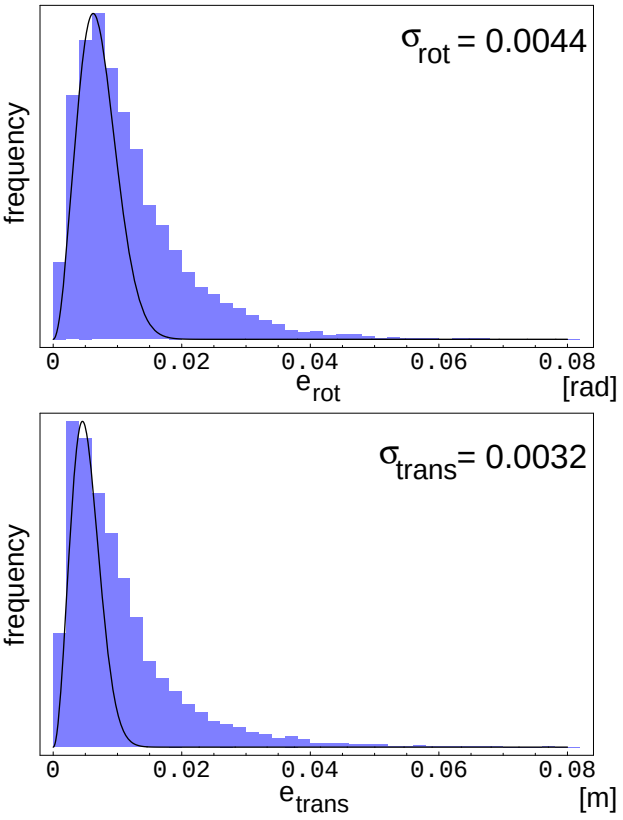

Fig. 9. Gaussian fits of estimation error for rotation (top) and translation (bottom) for the test-data sequences and scenario 3.

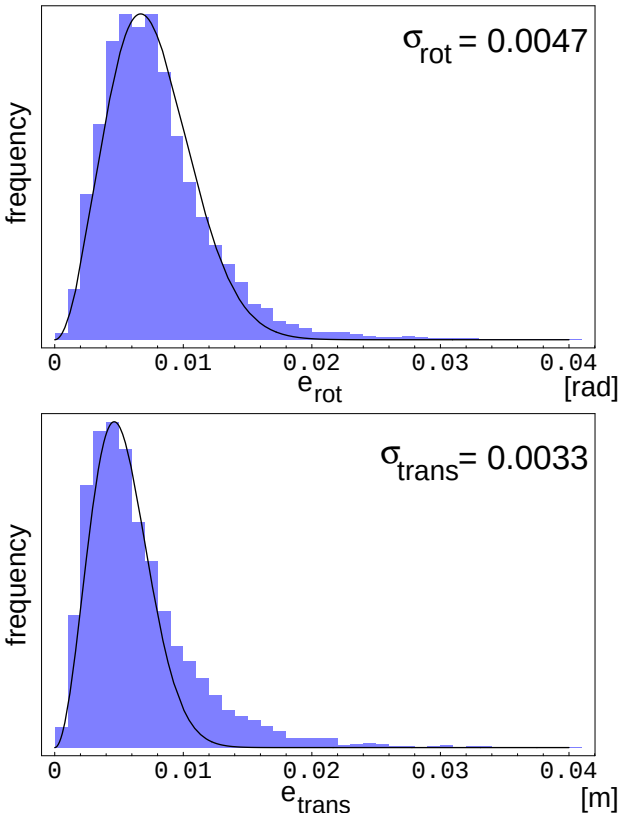

Fig. 8. Gaussian fits of estimation error for rotation (top) and translation (bottom) for the test-data sequences and scenario 2.

C. Motion prediction

Due to the prediction objective of this study, the error statistics for the identified dynamic parameters is not provided, but rather that of prediction errors. The error measure that is relevant to planning tasks such as grasping an object is the maximal pose error within the predicted time span. We have chosen a prediction time of 200 seconds, where the first 100 seconds coincide with the observation time.

The error for the predicted attitude is defined as

$$e_{\text{att}} = \max_{t\in[0,200]} ||\tilde{\alpha}(t) - \alpha(t)|| \ , \tag{38}$$

where $\alpha(t)$ is the canonical parameter vector of the absolute target orientation at time $t \in [0, 200]$ seconds, and $\tilde{\alpha}(t)$ is the predicted orientation; cf. eq. (32). We also consider the error of the predicted center-of-mass position,

$$e_{\text{cm}} = \max_{t\in[0,200]} ||\tilde{\mathbf{c}}(t) - \mathbf{c}(t)|| \ . \tag{39}$$

From 10 runs through each of the 10 trajectories we have obtained 100 samples of prediction errors for each of the three scenarios. Figures 10, 11, and 12 show frequency histograms of the attitude and center-of-mass errors.

The relation between the three sets of prediction errors reflects the relative results on motion estimation; cf. sec. IV-B. In particular, for scenario 1, 73% of the predictions are accurate within 20 deg and 10 cm for 100 seconds. For

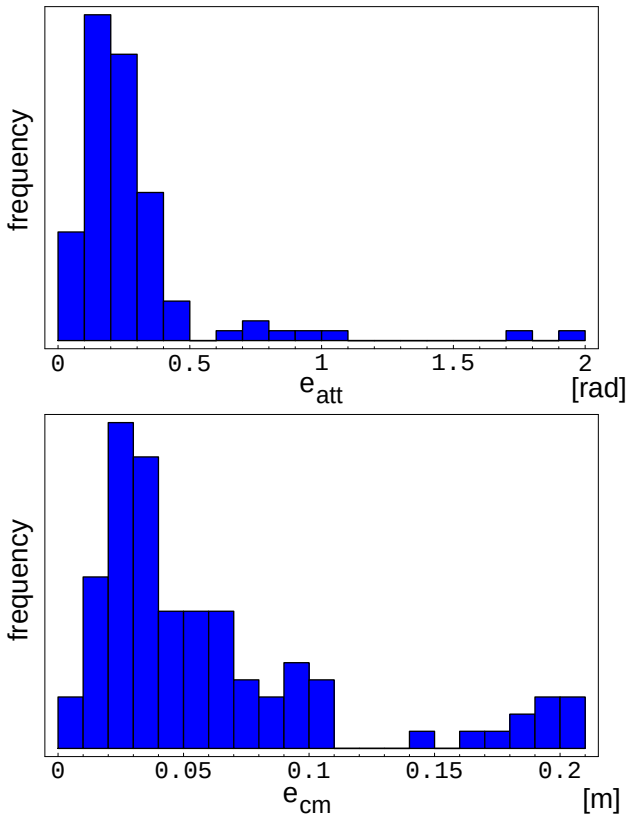

Fig. 10. Histograms of prediction error of target attitude (top) and center-of-mass position (bottom) for the test trajectories and scenario 1.

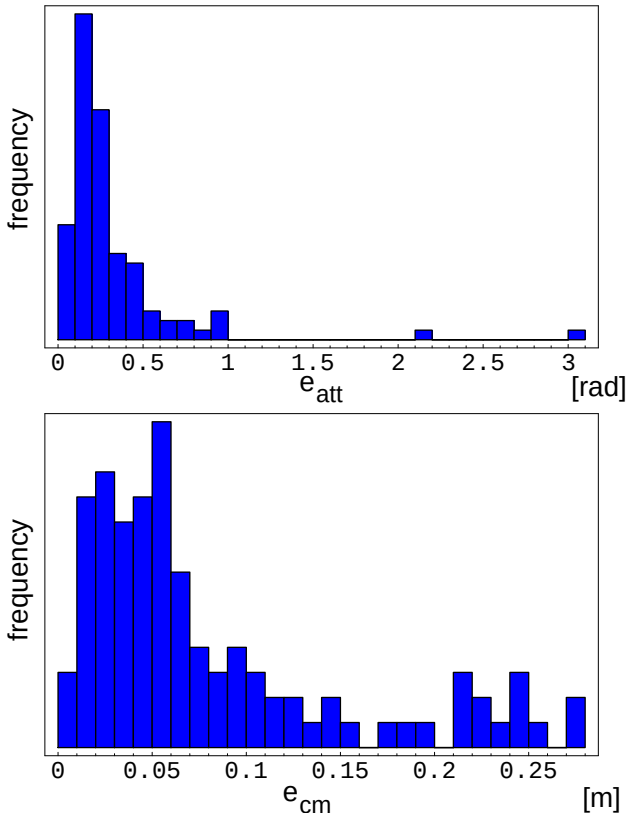

Fig. 11. Histograms of prediction error of target attitude (top) and center-of-mass position (bottom) for the test trajectories and scenario 2.

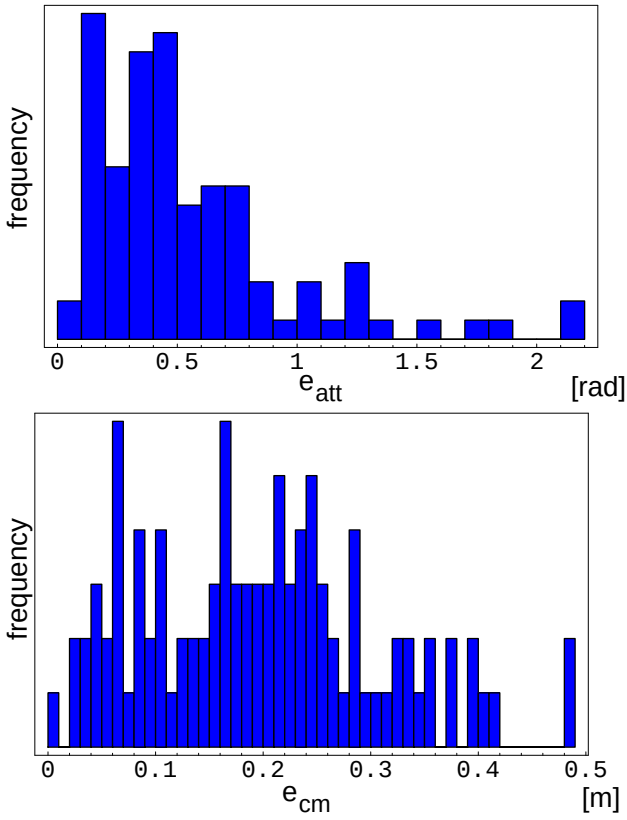

Fig. 12. Histograms of prediction error of target attitude (top) and center-of-mass position (bottom) for the test trajectories and scenario 3.

scenario 2, this proportion is still 52%, while for scenario 3, it drops to 13%.

In each scenario, there are some cases of dramatically wrong predictions, especially with regard to attitude. This has to do with the nonlinear dynamics of a rotating body, where trajectories may transiently pass through regimes with poor excitation of some of the rotational degrees of freedom. When observing the target in a phase of poor excitation, not all the inertial parameters may be well identifiable. If such parameters become influential for the observed or predicted trajectory at a later time, accurate prediction cannot be guaranteed. Figures 13 and 14 present a typical example of a successful prediction and a failure, respectively. Note that the prediction shown in Fig. 14 fails although, during the observation phase, the model matches as accurately as in the successful case of Fig. 13. The prediction fails because only one of the rotational degrees of freedom is significantly excited for the observed trajectory.

V. Conclusions

The method investigated for motion estimation proves able to track small motions with high precision. It turns out that the loss in estimation accuracy, brought about by not knowing point correspondences, is not dramatic. However, the case without point correspondences in the data proves a lot less suitable for long-term prediction, even with a 100-fold increase in data density. Moreover, the computation

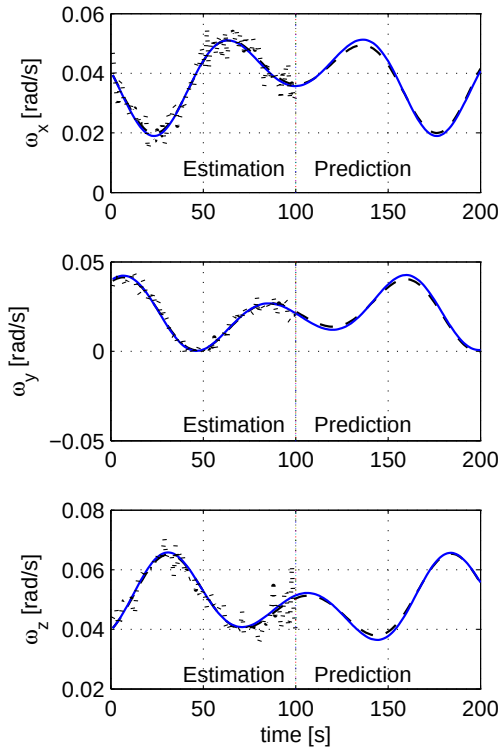

Fig. 13. Prediction example trajectory 1 (cf. table I); error = 0.2053; true motion: solid blue line; motion estimates: black dots; predicted motion: dashed black line.

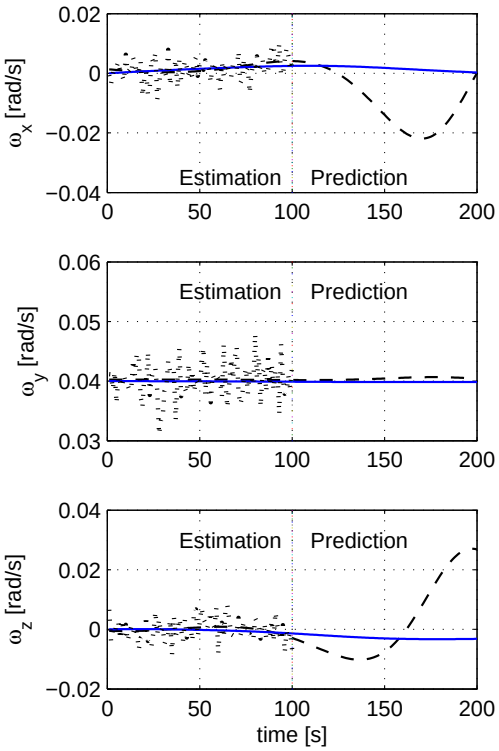

Fig. 14. Prediction example trajectory 2 (cf. table I); error = 1.9426; true motion: solid blue line; motion estimates: black dots; predicted motion: dashed black line.

time increases at least linearly with the number of data points, such that scenarios that can rely on few points are preferable.

The method investigated for the identification of dynamic model parameters has a computation time acceptable for a long-term prediction scenario and generally gives a reasonable output for motion prediction. However, due to the nonlinearity of the rotational dynamics, cases of insufficient prediction accuracy do occur. They are related to transiently poorly excited degrees of freedom in either observed or predicted trajectories. A principled approach to detecting a breakdown of prediction is to repeat the identification procedure many times, varying the initial guess, and checking the variation entailed for the predicted trajectory. In practice, however, the natural energy dissipation in the target structure (arising from flexible appendages etc.) is known to bring the target into a rotation about a stationary axis. Hence, a prediction such as shown in Fig. 14 can be rejected based on the sudden change of the angular velocity after the observation phase.

The procedure as a whole may prove valid to support predictive simulation for coarse planning of complex maneuvers such as autonomous grasping in many practical situations. Further analysis, including dependence on sampling rate or observation time, will allow to determine a minimum observation time which may ensure a desired statistical prediction accuracy for a given robotic task. Furthermore, using a range sensor with a better accuracy than 5 mm, will yield a higher prediction accuracy.

Evidently, the motion estimation procedure presented also yields a 3D reconstruction of the target (compare [2]) by accumulating the observed data in its body frame. Such a geometric model may be used subsequently for estimation of absolute pose and for contact planning.

REFERENCES

[1] Hirzinger, G., Landzettel, K., Fagerer, Ch.: *Telerobotics with large time delays - the ROTEX experience*, IEEE/RSJ International Conference on Intelligent Robots and Systems - IROS'94, Munich, Germany 1994.

[2] Lichter, M. D., Dubowsky, S.: *State, Shape and Parameter Estimation of Space Objects from Range Images*, IEEE International Conference on Robotics and Automation (ICRA 2004), New Orleans, LA, April 2004.

[3] Masutani, Y., Iwatsu, T., Miyazaki, F.: *Motion Estimation of Unknown Rigid Body under No External Forces and Moments*, IEEE International Conference on Robotics and Automation (ICRA 1994), San Diego, CA, May 1994.

[4] Greenspan, M., Shang, L., Jasiobedzki, P.: *Effi cient Tracking with the Bounded Hough Transform*, 2004 IEEE Computer Society Conference on Computer Vision and Pattern Recognition (CVPR'04), Volume 1, pp. 520-527.

[5] Horn, B. K. P.: *Closed-form solution of absolute orientation using unit quaternions*, J. Opt. Soc. Am. A **4** (1987), pp. 629–642.

[6] Eggert, D. W., Lorusso A., Fisher, R. B.: *Estimating 3-D rigid body transformations: a comparison of four major algorithms*, Mach. Vision App. **9** (1997), pp. 272–290.

[7] Besl, P.J., McKay, N.D.: *A method for registration of 3-D shapes*, IEEE Trans. Pattern Anal. Mach. Intell. **14** (1992), pp. 239–256.